The Structure of Mercury's Magnetic Field from MESSENGER's First Flyby

Brian J. Anderson, *et al.*

Science **321**, 82 (2008);
DOI: 10.1126/science.1159081

REPORT

The Structure of Mercury's Magnetic Field from MESSENGER's First Flyby

Brian J. Anderson,[1]* Mario H. Acuña,[2] Haje Korth,[1] Michael E. Purucker,[2] Catherine L. Johnson,[3] James A. Slavin,[4] Sean C. Solomon,[5] Ralph L. McNutt Jr.[1]

During its first flyby of Mercury, the MESSENGER spacecraft measured the planet's near-equatorial magnetic field. The field strength is consistent to within an estimated uncertainty of 10% with that observed near the equator by Mariner 10. Centered dipole solutions yield a southward planetary moment of 230 to 290 nanotesla R_M^3 (where R_M is Mercury's mean radius) tilted between 5° and 12° from the rotation axis. Multipole solutions yield non-dipolar contributions of 22% to 52% of the dipole field magnitude. Magnetopause and tail currents account for part of the high-order field, and plasma pressure effects may explain the remainder, so that a pure centered dipole cannot be ruled out.

Of the terrestrial planets, only Earth and Mercury possess global magnetic fields. The Mariner 10 encounters with Mercury in 1974 and 1975 (*1*–*3*) yielded the surprising result that Mercury has a coherent, intrinsic magnetic field (*4*–*6*). Estimates for the planetary dipole moment derived from Mariner 10 data range from 170 to 350 nT R_M^3 (where R_M is Mercury's mean radius); the uncertainty arises from the difficulty of distinguishing dipole and quadrupole contributions (*7*). Here, we apply magnetic field observations from the first MESSENGER flyby of Mercury (*8*, *9*) on 14 January 2008, herein M1, to determine the planetary moment and test for higher-order terms and secular changes in the internal field.

The spacecraft was within Mercury's magnetosphere for ~30 min during the flyby (Fig. 1). The inbound bow shock crossing corresponded to an abrupt increase in field magnitude, and the inbound magnetopause was evident in the decreased 1- to 10-Hz fluctuations and reduced directional and magnitude variability. At point A, the field rotated anti-sunward, azimuth near 180°, and the polar angle increased indicating passage out of the tail plasma sheet into the southern lobe. At point B, the 1- to 10-Hz fluctuations increased, indicating a change in local plasma conditions, and the field began to rotate northward at the same time that the magnitude increased, suggesting entry into a region dominated by the intrinsic field, interpreted here as departure from the southern tail lobe. Two field depressions occurred between B and closest approach (CA) with little corresponding change in field direction. There was a drop in field magnitude at point C, again without a change in direction. The outbound magnetopause boundary was indicated by the onset of large variations in magnitude and direction. Step C is interpreted elsewhere as a signature of a double magnetopause (*10*). At the outbound bow shock, the magnitude returned to the preencounter level. The interplanetary magnetic field (IMF) before and after the flyby was predominantly anti-sunward. There is no evidence of substormlike behavior or energetic particles (*10*). Thus, the M1 observations provide measurements of the magnetic field through an entire transit near the equator for undisturbed conditions.

To assess Mercury's intrinsic field, we applied spherical harmonic analysis (SHA) to the M1 observations combined with those from the first and third Mariner 10 flybys, M10-I and M10-III, respectively. The contribution of the external field must be considered because the magnetospheric fields are comparable to the planetary field (*11*, *12*). We used three approaches to the external field: (i) to gauge the

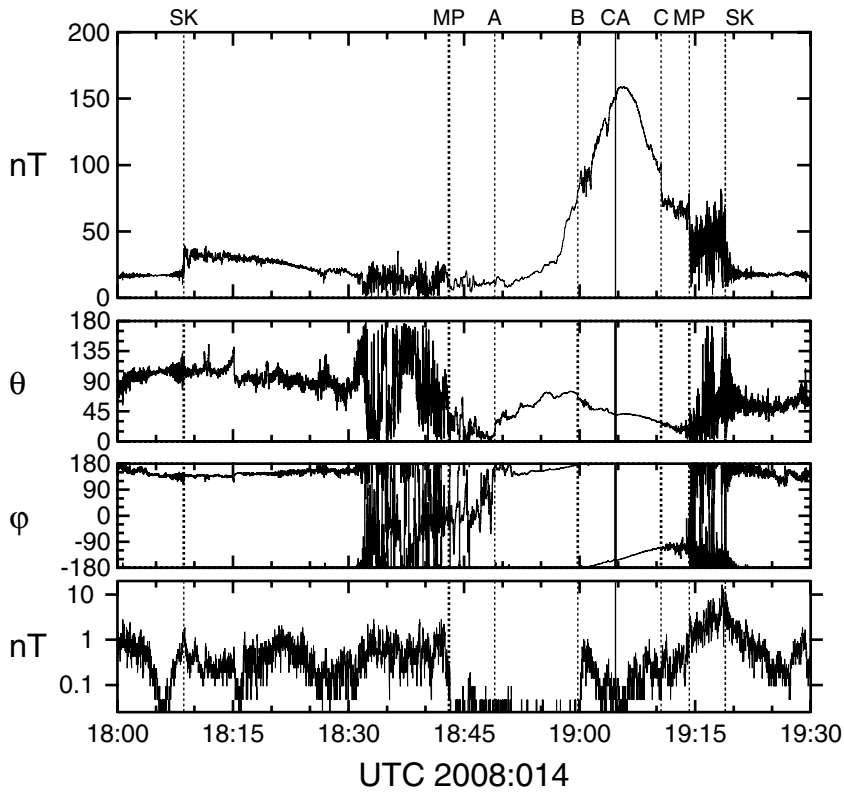

Fig. 1. MESSENGER Magnetometer observations for 14 January 2008 in polar Mercury solar orbital (MSO) coordinates versus UTC. θ is the polar angle (0° is north, normal to Mercury's orbital plane), and φ is azimuth (0° is sunward, 90° is duskward). Graphs show (**top**) field magnitude, (**middle**) θ and φ of the field direction, and (**bottom**) the 1- to 10-Hz bandpass fluctuation amplitude. Vertical lines indicate the bow shock crossings (SK), magnetopause crossings (MP), CA, and three transitions within Mercury's magnetosphere (A, B, and C). Data from B to C are used for intrinsic field analysis. Times (hh:mm:ss UTC) of the transitions are, for inbound SK, 18:08:38; inbound MP, 18:43:02; A, 18:52:04; B, 18:59:46; CA, 19:04:39; C, 19:10:34; outbound MP, 19:14:15; and outbound SK, 19:18:55.

[1]Johns Hopkins University Applied Physics Laboratory, 11100 Johns Hopkins Road, Laurel, MD 20723, USA. [2]Solar System Exploration Division, NASA Goddard Space Fight Center, Greenbelt, MD 20771, USA. [3]Department of Earth and Ocean Sciences, University of British Columbia, Vancouver, BC V6T 1Z4, Canada. [4]Heliophysics Science Division, NASA Goddard Space Flight Center, Greenbelt, MD 20771, USA. [5]Department of Terrestrial Magnetism, Carnegie Institution of Washington, Washington, DC 20015, USA.

*To whom correspondence should be addressed. E-mail: brian.anderson@jhuapl.edu

significance of subsequent corrections, we first ignored the external field; (ii) we used the empirical Tsyganenko and Sitnov (TS04) model (*13*), developed for Earth's magnetosphere and adapted for Mercury to include magnetopause and tail currents (*11*, *12*); and (iii) we allowed external coefficients in the SHA to estimate the external field from the data under the assumption that the region sampled was current-free (*14*).

The IMF and solar wind pressure inputs for the TS04 model were determined separately for each flyby. The IMF was taken to be the average over ~10 min in the solar wind near the bow shock, judged to best represent conditions near CA. For M1 and M10-III, we used data after the outbound bow-shock crossing. For M10-I, it was likely that the IMF changed during the encounter (*11*), so we used data before the first inbound shock crossing. The solar wind pressure was determined by fitting the outbound magnetopause crossing for each encounter (*12*). For the M10-I and M10-III data, we used the same data intervals that have been analyzed previously (*3*).

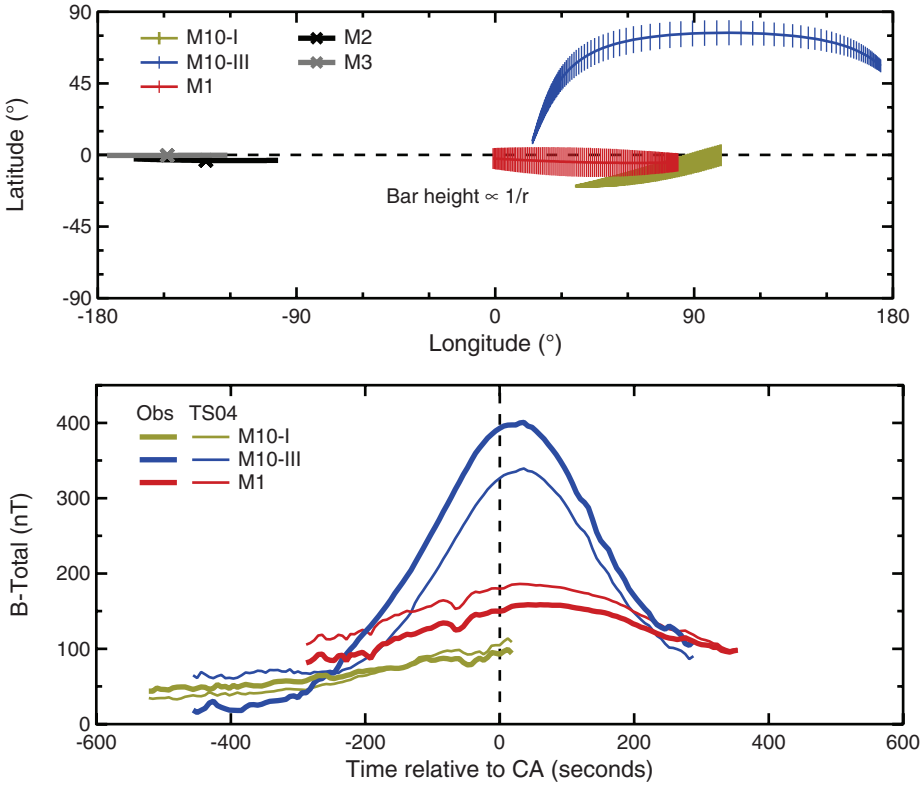

Fig. 2. Locations of all three encounters (**top**) and the field magnitude versus time relative to CA (**bottom**) for the intervals used in the analysis. The top graph shows latitude versus longitude for the M10-I, M10-III, and M1 encounters. Vertical bar heights are proportional to 1/*r*. The predicted latitude and longitude of the second and third MESSENGER flybys, M2 and M3, within 250 s of CA are also shown, where CA is indicated by crosses. In the bottom graph, thick lines show the raw data observations, and thin lines show observations with the TS04 external field subtracted.

Table 1. Dipole solutions to Mariner 10 and MESSENGER vector magnetic field data. A condition number (Cond. no.) lower than the ratio of the dipole moment to the root mean square deviation (RMSD) indicates a well-constrained solution. Δ_{xy} denotes the difference between solutions x and y; dipole magnitude (magn.) and direction (dir.).

Fit	External field approach	Data set(s)	Dipole (nT R_M^3)	Tilt	Longitude (north pole)	Condition number	RMSD (nT)
a	None	M10-I	−153	33°	−109°	2	15
b	None	M1	−168	17°	−135°	2	18
		Δ_{ab}	9% (magn.)		19° (dir.)		
c	TS04	M10-I	−197	18°	−29°	2	19
d	TS04	M1	−214	10°	−143°	2	11
		Δ_{cd}	8% (magn.)		24° (dir.)		
e	TS04	All	−229	9°	−161°	1	28
f	SHA 1 fit	All	−247	12°	−138°	10	26
g	SHA 3 fits	All	−290	5°	−161°	17	14
		Δ_{eg}	24% (magn.)		5.4° (dir.)		
		Δ_{fg}	16% (magn.)		7.1° (dir.)		

Determinations of the planetary field are influenced by the sampling coverage (Fig. 2). The M10-III observations were made near the northern pole, whereas M10-I and M1 measured the field near the equator. The maximum field magnitude recorded from M10-III was 401 nT, 2.5 times that observed from M1, 159 nT, even though CA for M10-III was at greater altitude than CA for M1, 327 km versus 201 km. This is not consistent with a centered dipole in vacuum because the maximum variation in field magnitude from a dipole is a factor of 2 at constant altitude.

The TS04-corrected values are more consistent with a dipole. The corrected field magnitude is lower for M10-III, higher for M1, and also higher for M10-I but only near CA, perhaps because the M10-I trajectory was at higher CA altitude (705 km). The magnetopause and tail currents reinforce the field over the pole and oppose the field near the equator on the nightside where CA for M1 and M10-I occurred, so correcting for the external field reduces the apparent pole-equator difference. The maximum magnitudes of the TS04-corrected fields are 339 nT for M10-III and 186 nT for M1. Scaling the value for M10-III from 330-km to 201-km altitude with a $1/r^3$ relation, where r is distance from the planet center, we estimated a maximum field at 201 km altitude near the north pole of 391 nT, 2.1 times greater than that observed during M1.

To assess whether the planetary moment changed since the Mariner 10 encounters, we compared observations from M10-I and M1, which followed similar trajectories. We evaluated the centered dipole separately from M10-I and M1 data with and without the TS04–external field correction (Table 1, fits a to d). The M10-I and M1 dipole results for the same external field correction agree to within 9% in magnitude and 24° in direction. Because results with and without the TS04–external field correction have comparable or greater differences, there is no statistically significant evidence for a change in the moment's magnitude or direction between 1974 and 2008.

Taking the intrinsic field to be unchanged, we used data from all three encounters to estimate the intrinsic field (fits e to g in Table 1). We calculated the SHA external field in two ways. First, we used data for the three encounters simultaneously to derive both the

planetary centered dipole and a single set of external-field coefficients to degree and order 2 (SHA 1). We also derived separate external SHA fits to degree and order 2 for each encounter while solving for a single dipole internal field (SHA 3). These solutions yielded a planetary moment of 229 to 290 nT R_M^3, directed southward, with a tilt between 5° and 12° from the rotation axis.

Structure in the field from orders higher than a centered dipole was assessed in two ways. First, we estimated spherical harmonic coefficients through degree and order 2 (*7*, *14*). Second, we used a regularized, constrained solution (Reg. TS04) through degree and order 6 in the internal field with the TS04 external field to minimize the unknowns. This method solves for higher-order spherical harmonic coefficients while minimizing the power in non-dipole terms. It applies a smoothness constraint on the power spectrum of the harmonics (*15*, *16*) by using a formalism that allows a data misfit tolerance and a damping of the model structure (*17*). The degree-6 solution used sufficient terms to ensure that the results were controlled by the smoothness constraint rather than truncation.

The results (Table 2 and Fig. 3) suggest that the pole-equator magnitude difference may be the principal factor driving the quadrupole term in the solutions. The dipole models (Fig. 3) illustrate that a centered dipole cannot account for the observed range in field magnitudes. The quadrupole solutions, I, III, and IV, have essentially the same north-south asymmetry, dipole magnitudes ($B_{n=1}$ of 210 to 227 nT), and higher-order terms ($B_{n>1}$ of 93 to 103 nT). The solution with no correction for the external field is similar to the two SHA external-field solutions. The SHA method for the external field thus had relatively little effect on the intrinsic field solution. Although solution IV yields the lowest deviation, the condition number implies that it is less well constrained than solutions I, II, or III.

The north-south asymmetry is reduced in the two solutions derived from TS04-corrected data. Although the dipole fit to the TS04-corrected data still cannot account for the remaining pole-equator difference in the field, the higher-order TS04 fits yield smaller quadrupole terms. Solutions II and V have lower $B_{n=1}$ and $B_{n>1}$, and, although their deviations are higher than the other solutions, the condition number for II is low. The relative contribution of higher-order terms in the regularized solution is less than half that of solution IV.

The small equatorial field relative to that observed near the pole results in quadrupole magnitudes that are ~45% of the dipole. Applying an external field correction that includes MP and tail currents accounts for some of this difference, but the inferred intensity at 200 km from M10-III is still 50 nT too large relative to the field at the equator to be explained with a centered dipole. The corresponding equatorial field deficit is ~25 nT.

The TS04 external field correction does not account for the effects of local plasma pressures in Mercury's magnetosphere (*18*). Two depressions in field intensity between B and CA (Fig. 1) have signatures consistent with local plasma pressure, one from 19:00 to 19:02 universal time coordinated (UTC) and the second near 19:04 UTC. Both are associated with increases in the proton plasma count rates (*18*). Interpreted as plasma pressure signatures, these correspond to increases

Table 2. Magnetic field amplitudes due to dipole and higher-order terms from intrinsic field solutions to combined Mariner 10 and MESSENGER vector field data. Field amplitudes $B_{n=1}$ and $B_{n>1}$ are the square roots of the spherical harmonic power evaluated at 200-km altitude for $n = 1$ and $n > 1$, where n denotes the degree in the spherical harmonic solution. For solutions I through IV, $B_{n>1}$ is the $n = 2$ (quadrupole) amplitude. For solution V, $B_{n>1}$ is the square root of the summed spectral power for $n = 2$ to 6. Fit V used a data misfit tolerance of 1.2 and a structure damping parameter of 0.01 (*17*). The condition number is not applicable (n/a) for solution V. Spherical harmonic coefficients through degree 2 are listed in table S1, which also lists the norm for the terms of degree 3 through 6 of solution V.

	Fit: External field and harmonic analysis technique				
	I None	II TS04	III SHA 1 fit	IV SHA 3 fits	V Reg. TS04
$B_{n=1}$ (nT)	254	199	249	235	212
$B_{n>1}$ (nT)	124	87	130	118	46
$B_{n>1}/B_{n=1}$	0.49	0.44	0.52	0.50	0.22
RMSD (nT)	17	25	17	7	24
Condition number	8	8	12	50	n/a

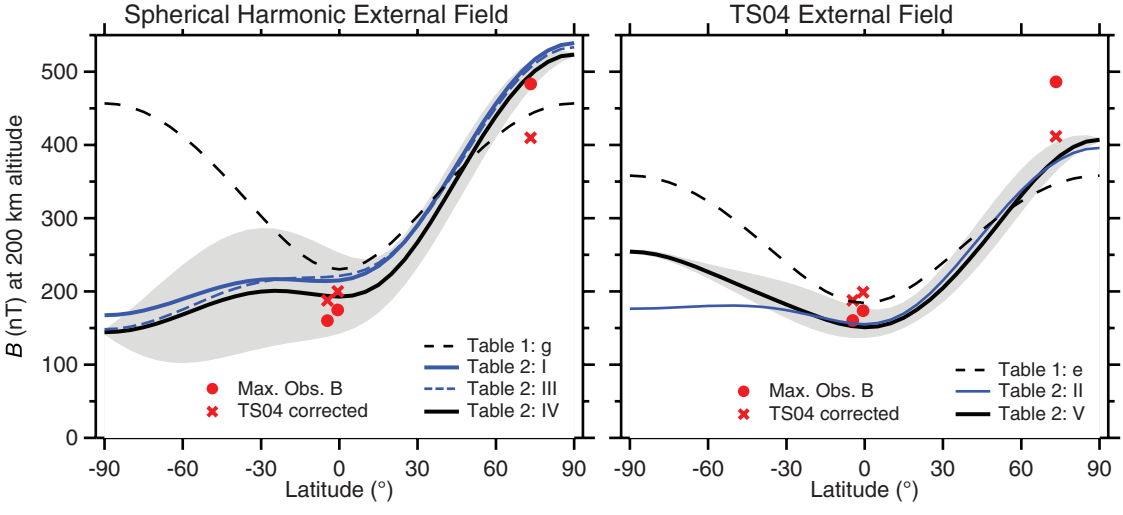

Fig. 3. Longitudinal averages versus latitude of 200-km-altitude magnetic field magnitudes from two classes of intrinsic field solutions as listed in Tables 1 and 2: those using either no external field or spherical harmonic representations for the external field (**left**) and those using the TS04 model adapted to Mercury (**right**). The observed magnitudes were mapped to 200 km with solution IV on the left and solution V on the right and by multiplying the observed magnitude by the ratio of the model field magnitude at 200 km and the observed altitude evaluated for the observation point latitude and longitude. As for the dipole inversions, we applied the SHA 1 and SHA 3 approaches to the spherical harmonic external field. In the left graph, the solid black line shows fit IV with gray shading indicating the range at a given latitude. Solid and dashed blue lines depict the results from fits I and III, respectively; and the dashed line shows the dipole fit g result. In the right graph, the solid black line shows fit V with gray shading as on the left, whereas the solid blue and dashed black lines show results from fits II and e, respectively. Red solid circles and crosses indicate the maximum magnetic field observed in each flyby extrapolated to 200 km.

in the plasma pressure of ~1.8 nPa. Also, coincident with the drop in field magnitude at C, the plasma proton count rates increased by a factor of three (*18*). The change in magnetic field magnitude implies a plasma pressure increase at C of ~2 nPa. Because the proton count rates before C were ~30% of those after C, the pressure before C was ~1 nPa, which would depress the field by ~7 nT.

Such signatures are consistent with hybrid simulations of Mercury's magnetosphere (*19*) that indicate an annulus of solar wind plasma within ~0.5 R_M altitude. The inward pressure gradient at the outer edge of such an annulus would suppress the magnetic field near the equator on the nightside and enhance it over the poles. The corresponding westward azimuthal current is about $I = hP/B$, where h is the vertical extent of the annulus, B is the magnetic field magnitude, P is the pressure in the annulus, and the pressure outside is taken to be zero. A 1-nPa pressure that goes to zero near 0.5 R_M altitude, where the field is ~50 nT, and that has a vertical extent of ~0.5 R_M corresponds to a current of 0.05 to 0.1 MA. This would decrease the equatorial field close to the planet by 10 to 30 nT and increase the field at the pole by ~5 to 10 nT. Thus, it is possible that the remaining deficit of equatorial field intensity of ~25 nT could be due to magnetospheric plasma. We conclude that an intrinsic quadrupole term is not required to account for the observations.

Recent simulations of Mercury's core dynamo suggest that the presence of a stagnant layer at the top of the molten outer core may suppress higher-order structure and yield secular variation over time scales of centuries rather than decades (*20*–*22*). We find no evidence for a change in the planetary dipole since 1974 and also find that the planetary field is predominantly and possibly entirely dipolar. Although there are significant uncertainties associated with these results, they are consistent with the presence of a stagnant outermost core.

References and Notes

1. N. F. Ness, K. W. Behannon, R. P. Lepping, Y. C. Whang, K. H. Schatten, *Science* **185**, 151 (1974).
2. N. F. Ness *et al.*, *J. Geophys. Res.* **80**, 2708 (1975).
3. N. F. Ness *et al.*, *Icarus* **28**, 479 (1976).
4. S. C. Solomon, *Icarus* **28**, 509 (1976).
5. L. J. Srnka, *Phys. Earth Planet. Inter.* **11**, 184 (1976).
6. D. J. Jackson, D. B. Beard, *J. Geophys. Res.* **82**, 2828 (1977).
7. J. E. P. Connerney, N. F. Ness, in *Mercury*, F. Vilas, C. R. Chapman, M. S. Matthews, Eds. (Univ. of Arizona Press, Tucson, 1988), pp. 494–513.
8. S. C. Solomon *et al.*, *Science* **321**, 59 (2008).
9. B. J. Anderson *et al.*, *Space Sci. Rev.* **131**, 417 (2007).
10. J. A. Slavin *et al.*, *Science* **321**, 85 (2008).
11. J. G. Luhmann *et al.*, *J. Geophys. Res.* **103**, 9113 (1998).
12. H. Korth *et al.*, *Planet. Space Sci.* **52**, 733 (2004).
13. N. A. Tsyganenko, M. I. Sitnov, *J. Geophys. Res.* **110**, A03208, 10.1029/2004JA010798 (2005).
14. D. Winch, in *Encyclopedia of Geomagnetism and Paleomagnetism*, D. Gubbins, E. Herrero-Bervera, Eds. (Springer, Dordrecht, Netherlands, 2007), pp. 448–452.
15. R. L. Parker, *Geophysical Inverse Theory* (Princeton Univ. Press, Princeton, NJ, 1994).
16. J. D. Bloxham *et al.*, *Philos. Trans. R. Soc. London Ser. A* **329**, 415 (1989).
17. C. J. Johnson, C. G. Constable, *Geophys. J. Int.* **122**, 489 (1995).
18. T. H. Zurbuchen *et al.*, *Science* **321**, 90 (2008).
19. P. Trávníček *et al.*, *Geophys. Res. Lett.* **34**, L05104, 10.1029/2006GL028518 (2007).
20. U. R. Christensen, *Nature* **444**, 1056 (2006).
21. F. Takahashi, M. Matsushima, *Geophys. Res. Lett.* **33**, L10202 10.1029/2006GL025792 (2006).
22. J. Wicht *et al.*, *Space Sci. Rev.* **132**, 261 (2007).

23. The MESSENGER project is supported by the NASA Discovery Program under contracts NAS5-97271 to Johns Hopkins University Applied Physics Laboratory and NASW-00002 to the Carnegie Institution of Washington. Support was also provided under the NASA MESSENGER Participating Science Program via grant NNX07AR73G.

14 April 2008; accepted 6 June 2008
10.1126/science.1159081

REPORT

Mercury's Magnetosphere After MESSENGER's First Flyby

James A. Slavin,[1]* Mario H. Acuña,[2] Brian J. Anderson,[3] Daniel N. Baker,[4] Mehdi Benna,[2] George Gloeckler,[5,6] Robert E. Gold,[3] George C. Ho,[3] Rosemary M. Killen,[6] Haje Korth,[3] Stamatios M. Krimigis,[3,7] Ralph L. McNutt Jr.,[3] Larry R. Nittler,[8] Jim M. Raines,[5] David Schriver,[9] Sean C. Solomon,[8] Richard D. Starr,[10] Pavel Trávníček,[11] Thomas H. Zurbuchen[5]

Observations by MESSENGER show that Mercury's magnetosphere is immersed in a comet-like cloud of planetary ions. The most abundant, Na^+, is broadly distributed but exhibits flux maxima in the magnetosheath, where the local plasma flow speed is high, and near the spacecraft's closest approach, where atmospheric density should peak. The magnetic field showed reconnection signatures in the form of flux transfer events, azimuthal rotations consistent with Kelvin-Helmholtz waves along the magnetopause, and extensive ultralow-frequency wave activity. Two outbound current sheet boundaries were observed, across which the magnetic field decreased in a manner suggestive of a double magnetopause. The separation of these current layers, comparable to the gyro-radius of a Na^+ pickup ion entering the magnetosphere after being accelerated in the magnetosheath, may indicate a planetary ion boundary layer.

The interaction of Mercury's magnetic field with the solar wind creates a small magnetosphere with a typical standoff altitude of ~0.5 R_M (where R_M is the mean planet radius; 1 R_M ~ 2440 km) (*1*, *2*) (Fig. 1). The MESSENGER spacecraft made the first of three flybys of Mercury on 14 January 2008 (*3*) and took measurements within Mercury's magnetosphere with its magnetometer (MAG) (*4*, *5*); energetic particle and plasma spectrometer, composed of the energetic particle spectrometer (EPS) and fast imaging plasma spectrometer (FIPS) (*6*, *7*); and x-ray spectrometer (XRS) (*8*).

The presence of the magnetosphere as an obstacle to the solar wind is signaled by the bow shock (BS), which was crossed at 18:08:38 (inbound) and 19:18:55 (outbound). Before the inbound magnetopause (MP) crossing at 18:43:02, the last extended interval of southward interplanetary magnetic field (IMF) ended at 18:38:40. The magnetosheath magnetic field was observed to be generally northward after the exit from the magnetosphere at 19:14:15. A northward IMF is unfavorable to dayside magnetic reconnection with Mercury's magnetic field and greatly limits the rate of solar wind energy transfer across the

[1]Heliophysics Science Division, NASA Goddard Space Flight Center, Greenbelt, MD 20771, USA. [2]Solar System Exploration Division, NASA Goddard Space Fight Center, Greenbelt, MD 20771, USA. [3]Johns Hopkins University Applied Physics Laboratory, Laurel, MD 20723, USA. [4]Laboratory for Atmospheric and Space Physics, University of Colorado, Boulder, CO 80303, USA. [5]Department of Atmospheric, Oceanic, and Space Sciences, University of Michigan, Ann Arbor, MI 48109, USA. [6]Department of Astronomy, University of Maryland, College Park, MD 20742, USA. [7]Academy of Athens, Athens 11527, Greece. [8]Department of Terrestrial Magnetism, Carnegie Institution of Washington, Washington, DC 20015, USA. [9]Institute of Geophysics and Planetary Physics, University of California, Los Angeles, CA 90024, USA. [10]Department of Physics, Catholic University of America, Washington, DC 20064, USA. [11]Astronomical Institute, Academy of Sciences of the Czech Republic, Prague, Czech Republic.

*To whom correspondence should be addressed. E-mail: james.a.slavin@nasa.gov